

INVESTIGATION OF THE SPATIAL VARIABILITY OF SEISMIC INPUT MOTIONS FOR CSMIP-INSTRUMENTED BRIDGES DURING THE 2014 SOUTH NAPA EARTHQUAKE—THE CASE OF GOLDEN GATE BRIDGE

S. F. Ghahari¹, H. Ebrahimian² and E. Taciroglu¹

¹Department of Civil & Environmental Engineering, University of California, Los Angeles

²Department of Mechanical and Civil Engineering, California Institute of Technology

Abstract

This paper presents interim results from a study on the identification of spatial variability in bridge Foundation Input Motions (FIMs) observed during the 2014 South Napa Earthquake. Bridges are especially prone to the spatial variability of ground motions because they extend over relatively long distances. The primary objective of this project has been to develop a framework to identify FIMs from response signals recorded at instrumented bridges, because, in general, FIMs cannot be measured directly. In this progress paper, we present the development and verification of a framework developed for this purpose and its application to a real-life case study—namely, the Golden Gate Bridge. This bridge was chosen, because initial analysis suggested that its behavior is not significantly affected by inertial soil-structure interaction effects, and thus, the identified FIMs could be—at least partially—validated. Results obtained from both verification (identification using simulated response signals) and validation (identification using real-life data) confirmed the applicability of the developed framework, which will be applied to the other long-span bridges affected by the 2014 South Napa Earthquake in a follow-up study.

Introduction

In order to accurately estimate the response of bridge structures under earthquake ground motions, highly detailed and accurate Finite Element (FE) models are necessary; but they are not sufficient by themselves. While presently available commercial/open-source software packages enable accurate response predictions for bridges, our inability to apply physically accurate/consistent input motions remains a major challenge. This issue is even more challenging for long-span bridges due to the *spatial variability* of input motions [1]. In current practice, California Department of Transportation (Caltrans), for example, takes spatial variability into account by computationally producing ground motions at each pier of the bridge using one-dimensional site-response analyses. That is, the seismic motion estimated on the bedrock is transferred to the surface at each pier using specific soil properties at each pier's site. In the presence of kinematic Soil-Structure Interaction (SSI) effects, these Free-Field Motions (FFMs) must also be converted to the so-called Foundation Input Motions (FIMs) (see **Figure 1**). Therefore, while ground motions at the bedrock of the bridge site may be uniform, a long bridge may still experience differing excitations at different piers. This procedure assumes vertically propagating horizontally polarized waves, which is not necessarily true. The deconvolution procedures used for estimating the bedrock motions from ground surface records also introduce various numerical errors (including unrealistically large motions at the bedrock). Conversion of

FFMs into FIMs is another source of potentially significant error, and at the present time, there is no validated procedure to carry out the said conversion.

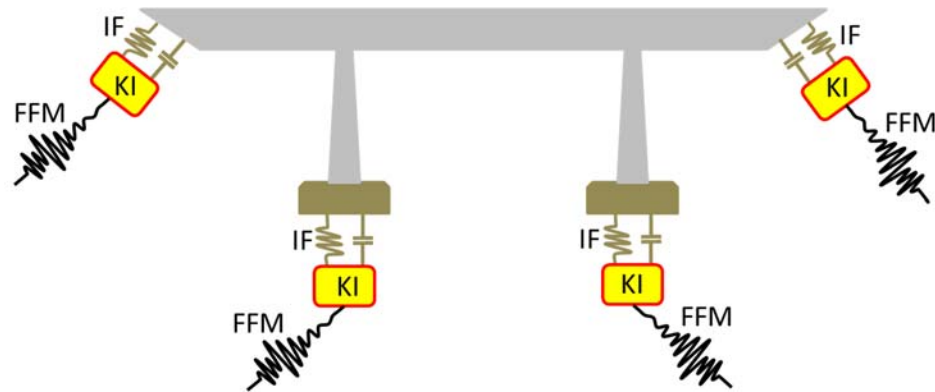


Figure 1. Schematic representation of dynamic analysis of a long bridge.

The back-calculation of FIMs from real-life data is a key capability to study spatial variability effects and to validate (or to refute) new or existing procedures that predict the foundation input motions. In our previous study [2], we showed some evidences of spatial variability in data recorded on the foundation level of bridges during 2014 South Napa earthquake. However, due to possible inertial soil-structure interaction effects, these foundation level measurements may not be representative of FIMs. To resolve this issue, we proposed a framework to recover FIMs from recorded response of bridge structures instrumented through California Strong Motion Instrumentation Program (CSMIP) [3]. In the present paper, we verify and validate the proposed framework through both simulation and real-life data obtained from the Golden-Gate Bridge. There is almost no overlap between this paper and our previous study in SMIP16, so the readers should refer to [2] for more details about the definitions, objective, and overall plan. Also, the methods developed to recover bedrock motion and site effect transfer function from identified FIMs are discussed in [2] which are not discussed here for the sake of space. Details of these methods can be found in [4] and [5].

Data Selection

As mentioned above, this project will use data recorded during the 2014 South Napa earthquake. To be able to select earthquake data sets in systematic way, a Matlab [6] toolbox, called CSMIP-BRIDGE, is developed, which is able to connect to the Center for Engineering Strong Motion Data (CESMD)¹ [7], collects meta data of all bridges instrumented through CSMIP. An overview of this toolbox is shown in **Figure 2**. Current version of this toolbox has a database which can be updated manually by the user. Also, there is search form through which bridges with specific characteristics can be identified. As seen in **Figure 2**, currently there are 81 instrumented bridges in the database. 17 of the 80+ instrumented bridges recorded the South Napa earthquake. In our previous study [2], we described a process through which 7 bridges (CSMIP 68184, 68185, 68322, 68682, 58632, 58700, and 67771) can be subject of the current

¹ www.strongmotioncenter.org

project based on some criteria like level of vibration, sensor distribution, having nearby FFM, etc.

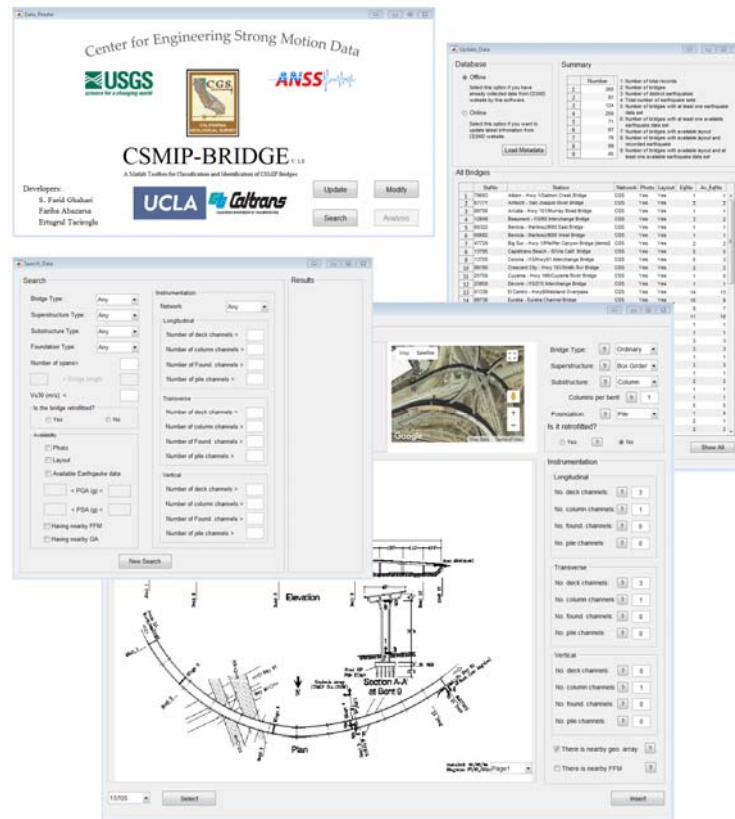


Figure 2. CSMIP-BRIDGE toolbox.

Identification Method

Our objective is to estimate jointly the model parameters and the time history of the foundation input motions (FIMs) using the recorded dynamic response of a bridge structure during an earthquake. For this purpose, we adopted the output-only Extended Kalman Filter (EKF) presented by Huang et al. [8] in our SMIP16 paper [2]. We successfully verified that approach through a simple 39-DOF synthetic example shown in **Figure 3** where 6 parameters of the structure (modules of elasticity of the deck beam, two Rayleigh damping parameters, and three soil-foundation springs) along with three FIMs were unknown. We were able to identify unknown parameters and FIMs with measured response simulated at only five locations as shown in **Figure 4** and **Figure 5**, respectively. However, that method is not suitable for real-life structures that exhibit significant nonlinearities (material and/or geometry). In the present study, we have developed a joint parameter and input estimation approach based on the unscented Kalman filtering method [9]. The estimation approach is briefly described in this section.

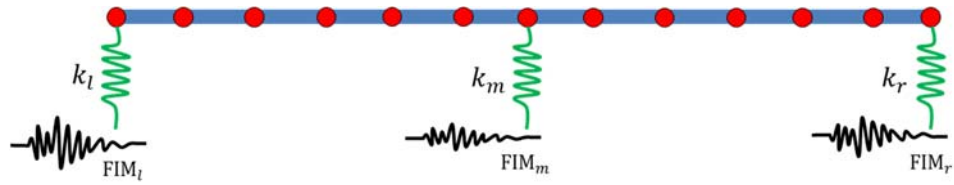


Figure 3. Synthetic bridge model with multiple support excitation.

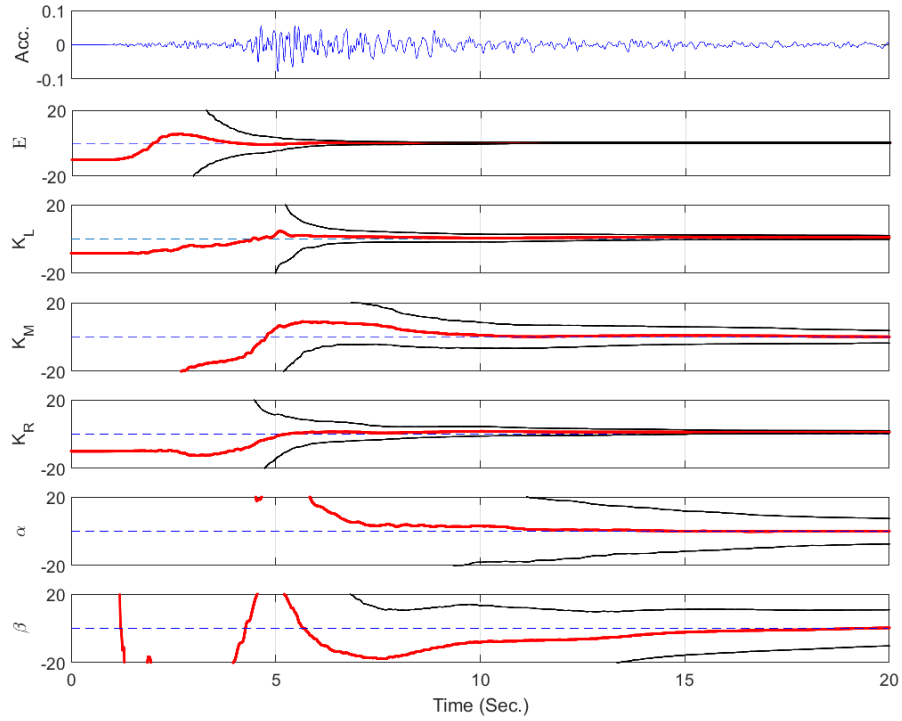


Figure 4. Error convergence rate.

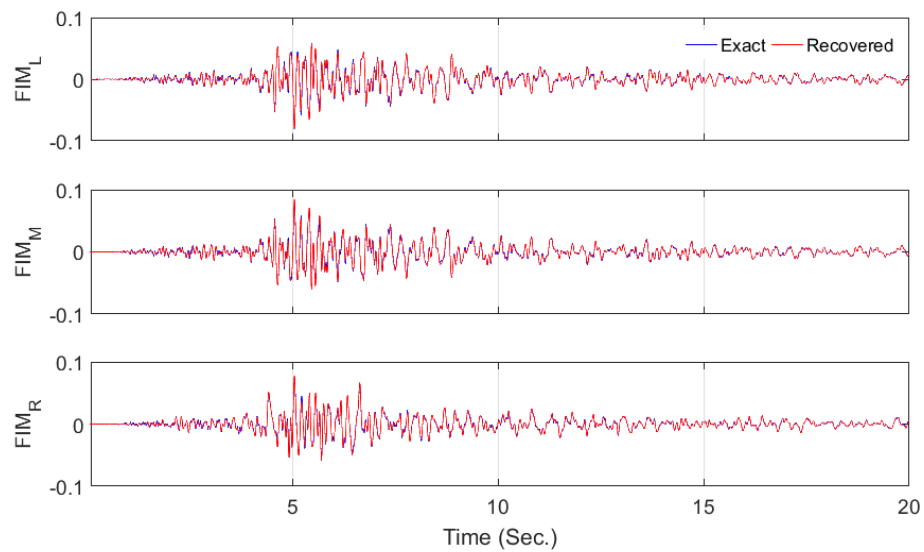


Figure 5. Comparison between exact and identified FIMs.

The response of the Finite Element (FE) model of a bridge structure at each time step to a multi-support earthquake excitation can be expressed as a (nonlinear) function of the model parameter vector, $\boldsymbol{\theta}$, and the time history of the base input motions, $\ddot{\mathbf{u}}_{1:i}^g$, i.e.,

$$\hat{\mathbf{y}}_i = h_i(\boldsymbol{\theta}, \ddot{\mathbf{u}}_{1:i}^g), \quad 1)$$

where $h_i(\cdot)$ is the nonlinear response function of the FE model at time step i , encapsulating all the dynamics of the model from time step 1 to i . The measured response vector of the structure, \mathbf{y}_i , is related to the FE predicted response, $\hat{\mathbf{y}}_i$, as

$$\mathbf{v}_i(\boldsymbol{\theta}, \ddot{\mathbf{u}}_{1:i}^g) = \mathbf{y}_i - \hat{\mathbf{y}}_i(\boldsymbol{\theta}, \ddot{\mathbf{u}}_{1:i}^g), \quad 2)$$

in which $\mathbf{v}_i \in \mathbb{R}^{n_y \times 1}$ is the simulation error vector and accounts for the misfit between the measured and FE predicted response of the structure. The simulation error is ideally modeled as a zero-mean Gaussian white noise vector (i.e., $\mathbf{v}_i \sim N(\mathbf{0}, \mathbf{R})$) by neglecting the effects of modeling error [10]. The objective of the estimation problem is to find the estimates of the unknown parameter vector, i.e., $\boldsymbol{\psi}_i = [\boldsymbol{\theta}^T, \ddot{\mathbf{u}}_{1:i}^{g,T}]^T$, for which the discrepancies between the measured and FE predicted responses are minimized in a probabilistic sense. Since the estimation problem is highly nonlinear, a sequential estimation approach is used in this study to improve the estimation efficiency. In this approach, the time domain is divided into successive overlapping time windows, referred to as the estimation windows. The estimation problem is solved at each estimation window to estimate the unknown parameter vector. Assume that the m -th estimation window spans from time step t_1^m to time step t_2^m . Therefore, the unknown parameter vector at this estimation window is defined as $\boldsymbol{\psi}_m = [\boldsymbol{\theta}^T, \ddot{\mathbf{u}}_{t_1^m:t_2^m}^{g,m,T}]^T$, where $\boldsymbol{\psi}_m \in \mathbb{R}^{(n_\theta + t_l \times n_{\ddot{\mathbf{u}}^g}) \times 1}$, in which $t_l = t_2^m - t_1^m$ is the estimation window length, and $n_{\ddot{\mathbf{u}}^g}$ is the number of unknown components of the base input motions. The unknown parameter vector, $\boldsymbol{\psi}_m$, is estimated using a parameter-only Kalman filtering method. To this end, the unknown parameter vector is modeled as a random vector, the evolution of which is characterized by a Gaussian Markov process – also known as a random walk. Then, a state space model is set up, in which the state equation governs the evolution of the random parameter vector and the measurement equation corresponds to the discrepancies between the measured and FE predicted structural responses [11], i.e.,

$$\boldsymbol{\psi}_{m,k+1} = \boldsymbol{\psi}_{m,k} + \boldsymbol{\gamma}_{m,k}, \quad 3)$$

$$\mathbf{y}_{t_1^m:t_2^m} = \hat{\mathbf{y}}_{t_1^m:t_2^m,k+1}(\boldsymbol{\psi}_{m,k+1}) + \mathbf{v}_{t_1^m:t_2^m,k+1}, \quad 4)$$

in which $\boldsymbol{\gamma}_{m,k} \sim N(\mathbf{0}, \mathbf{Q})$, $\mathbf{v}_{t_1^m:t_2^m,k+1} \sim N(\mathbf{0}, \tilde{\mathbf{R}})$, where $\tilde{\mathbf{R}} \in \mathbb{R}^{(t_l \times n_y) \times (t_l \times n_y)}$ is a block diagonal matrix, whose block diagonals are the simulation error covariance matrix \mathbf{R} . In Eqs. (3) and (4), k denotes the iteration number. As can be observed, the estimation process at each estimation window is iterative, i.e., the mean vector and covariance matrix of the unknown parameter vector is iteratively updated based on the discrepancies between the time histories of the measured and estimated responses.

An Unscented Kalman Filtering (UKF) method is used to update the unknown parameter vector at each iteration. In this method, the nonlinear FE model is evaluated separately at a set of

deterministically selected realizations of the unknown parameter vector, which are referred to as the sigma points (SPs) denoted by $\boldsymbol{\vartheta}^j$. The sigma points are selected around the prior mean estimate $\widehat{\boldsymbol{\psi}}^-$. In this study, a scaled Unscented Transformation (UT) based on $2n_\psi + 1$ sigma points (i.e., $j = 1, 2, \dots, 2n_\psi + 1$) is used, where n_ψ denotes the size of the extended parameter vector. The mean and covariance matrix of the FE predicted structural responses, and the cross-covariance matrix of $\boldsymbol{\psi}$ and \mathbf{y} are respectively computed using a weighted sampling method as

$$\bar{\mathbf{y}} = \sum_{j=1}^{2n_\psi+1} W_m^j \widehat{\mathbf{y}}_i(\boldsymbol{\vartheta}^j), \quad (5)$$

$$\widehat{\mathbf{P}}_{yy} = \sum_{j=1}^{2n_\psi+1} W_e^j [\widehat{\mathbf{y}}_i(\boldsymbol{\vartheta}^j) - \bar{\mathbf{y}}][\widehat{\mathbf{y}}_i(\boldsymbol{\vartheta}^j) - \bar{\mathbf{y}}]^T + \mathbf{R}, \quad (6)$$

$$\widehat{\mathbf{P}}_{\psi y} = \sum_{j=1}^{2n_\psi+1} W_e^j [\boldsymbol{\vartheta}^j - \widehat{\boldsymbol{\psi}}^-][\widehat{\mathbf{y}}_i(\boldsymbol{\vartheta}^j) - \bar{\mathbf{y}}]^T, \quad (7)$$

where W_m^j and W_e^j denote weighting coefficients [12]. Now, the UKF prediction-correction procedure can be employed to estimate the posterior parameter mean vector $\widehat{\boldsymbol{\psi}}^+_{m,k+1}$ and covariance matrix $\widehat{\mathbf{P}}^+_{\psi,m,k+1}$ at each iteration. The identification algorithm is summarized in **Table 1**.

Table 1. Identification algorithm for joint estimation of the model parameters and the FIM time history.

<p>1. Set the estimation window length t_l, and the start and end points of each estimation window.</p> <p>2. Set the initial mean vector and covariance matrix of the unknown parameter vector as</p> $\widehat{\boldsymbol{\psi}}^+_0 = [\widehat{\boldsymbol{\theta}}_0^T, \widehat{\mathbf{u}}_{t_1^0:t_2^0}^{g,0}{}^T]^T, \text{ and } \mathbf{P}^+_{\psi,0} = \begin{bmatrix} \widehat{\mathbf{P}}_{\theta\theta,0} & \mathbf{0} \\ \mathbf{0} & \widehat{\mathbf{P}}_{\mathbf{u}^{g,0}} \end{bmatrix}.$ <p>3. Define the process noise covariance matrix \mathbf{Q} and the simulation error covariance matrix \mathbf{R}. Set up matrix $\widetilde{\mathbf{R}}$.</p> <p>4. For the m-th estimation window:</p> <p>4.1. Retrieve the posterior estimates of the mean vector and covariance matrix of the unknown parameter vector from the last estimation window (i.e., $\widehat{\boldsymbol{\psi}}^+_{m-1}$, and $\mathbf{P}^+_{\psi,m-1}$). Set up $\widehat{\boldsymbol{\psi}}^+_{m,0}$ and $\mathbf{P}^+_{\psi,m,0}$ based on $\widehat{\boldsymbol{\psi}}^+_{m-1}$ and $\mathbf{P}^+_{\psi,m-1}$.</p> <p>4.2. Iterate ($k = 1, 2, \dots$):</p> <p>a. Set $\widehat{\boldsymbol{\psi}}^-_{m,k+1} = \widehat{\boldsymbol{\psi}}^+_{m,k}$, $\mathbf{P}^-_{\psi,m,k+1} = \mathbf{P}^+_{\psi,m,k} + \mathbf{Q}$.</p> <p>b. Generate sigma points. Run the FE model for $(2n_\psi + 1)$ sigma points. Derive $\bar{\mathbf{y}}$, $\widehat{\mathbf{P}}_{yy}$, and $\widehat{\mathbf{P}}_{\psi y}$ using Eqs. (5)-(7).</p> <p>c. Compute the Kalman gain matrix: $\mathbf{K} = \widehat{\mathbf{P}}_{\psi y}(\widehat{\mathbf{P}}_{yy})^{-1}$.</p> <p>d. Find the corrected estimates of the mean vector and covariance matrix of the unknown parameter vector:</p> $\widehat{\boldsymbol{\psi}}^+_{m,k+1} = \widehat{\boldsymbol{\psi}}^-_{m,k+1} + \mathbf{K}(\mathbf{y}_{t_1^m:t_2^m} - \bar{\mathbf{y}}), \mathbf{P}^+_{\psi,m,k+1} = \mathbf{P}^-_{\psi,m,k+1} - \mathbf{K}(\widehat{\mathbf{P}}_{yy} + \widetilde{\mathbf{R}})\mathbf{K}^T.$ <p>e. Check for convergence: if $\widehat{\boldsymbol{\psi}}^+_{m,k+1} - \widehat{\boldsymbol{\psi}}^+_{m,k} < 0.02 \times \widehat{\boldsymbol{\psi}}^+_{m,k-1}$ or $k + 1 > 10$, then move to the next estimation window ($m = m + 1$, go to step 4); otherwise, iterate again at the current estimation window ($k = k + 1$, go to step 4.2).</p>
--

Verification and Validation

To verify and validate output-only identification method, we use both simulated and real-life data obtained from the Golden Gate Bridge (GGB), respectively. GGB is chosen for this pilot study because it was the only bridge with structural drawings available to us at the present time. Also, we expected to have negligible inertial SSI effects due to the flexibility of the bridge, so foundation responses would be representative of FIMs and thus could be used to validate the identified FIMs.

The Structural System

The Golden Gate (**Figure 6**) is a strait that connects the San Francisco Bay to the Pacific Ocean. The GGB is a suspension bridge over Golden Gate, which connects San Francisco to Marin County. GGB was the longest (main span) suspension bridge in the world until 1964. It has been also declared one of the wonders of the modern world by the American Society of Civil Engineers (ASCE).



Figure 6. Golden Gate.

The GGB was completed and opened to traffic on May 28, 1937 [13]. The total length of the GGB from abutment to abutment is 2737 m (8981 ft), with other detailed dimensions of the bridge as shown in **Figure 7**. Summarizing from [14], the structural system is briefly reviewed here (Geometrical and mechanical properties of these elements can be found, for example, in [15], [16] and not discussed here for brevity). As a suspension bridge, the GGB consists of several structural systems. To have a visual understating, **Figure 8** is presented. The approach viaducts are of steel girder, truss and arch construction. Anchorage blocks (south one is not shown in **Figure 8**), piers, and pylons are of reinforced concrete construction. The towers, deck, and cables (main cable and hangers) are of steel construction. The towers are founded directly on the underlying rock. The deck, which was originally of reinforced concrete and replaced by orthotropic steel plate at the center and reinforced concrete sidewalks in 1980's, is carried on floor beams every 25 ft. These beams are connected to stiffening trusses at both sides. In original construction, stiffening trusses were connected to each other with only a top lateral bracing system. Later, in 1950's, a bottom lateral bracing system was added to make the roadway

supporting system a closed box and consequently reduce deck's torsion/twist. The entire mentioned stiffening system is suspended every 50 ft with hangers on each side, were replaced in 1970's. The main span is fixed laterally and vertically to the towers at its both ends, has a limited amount of free movement in the longitudinal direction, and fully released for rotation at its both ends through joints.

While the GGB has experienced several retrofit stages as mentioned above, prompted by the 1989 Loma Prieta earthquake, the GGB, Highway and Transportation District² initiated a series of studies of the bridge which concluded necessity of a massive retrofit including [17]:

- installation of dampers between the stiffening trusses and the towers,
- replacement of one-quarter of the stiffening truss lateral braces with new ductile members,
- stiffening of the bridge towers to prevent undesirable plate buckling,
- strengthening of the bridge piers,
- strengthening of the saddles supporting cables on the tops of the towers,
- strengthening of the wind-locks connecting the suspended structure and the towers,
- and strengthening of the pedestals supporting the orthotropic deck.

The retrofit started in 1997 and was initially planned to be ended in 2012, which was later changed several times (lately to 2021). Retrofit carried out in three phases due to several factors like level of vulnerability, provided fund, and traffic closure. In Phase 1 (1997-2002), the Marin (North) approach viaduct was retrofitted. In Phase 2 (2002-2007), San Francisco (South) approach viaduct, anchorage housing, arch, and pylons were retrofitted. Phase 3 (2008-2021) was conducted in two sub phases A and B. In Phase 3A (2008-2014), North Anchorage housing and pylon were retrofitted. In Phase 3B, main suspension span, main towers, South tower pier and fender is going to be retrofitted. This phase is the most challenging part and mainly due to this reason the completion date of retrofit project has been extended to 2021. Another reason for such extension was to increase the strength of the bridge against factors beyond earthquakes, like terrorism attacks. As a summary, details of the retrofit measures conducted at each phase are shown in **Figure 9**.

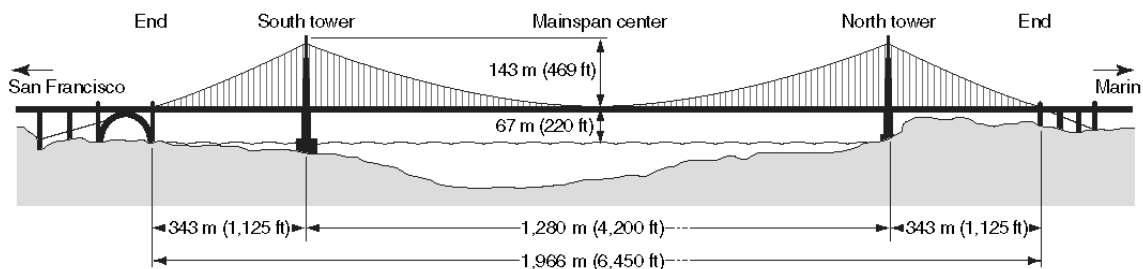


Figure 7. Dimensions of the bridge [18].

² This is a special district of the state of California formed in 1928.

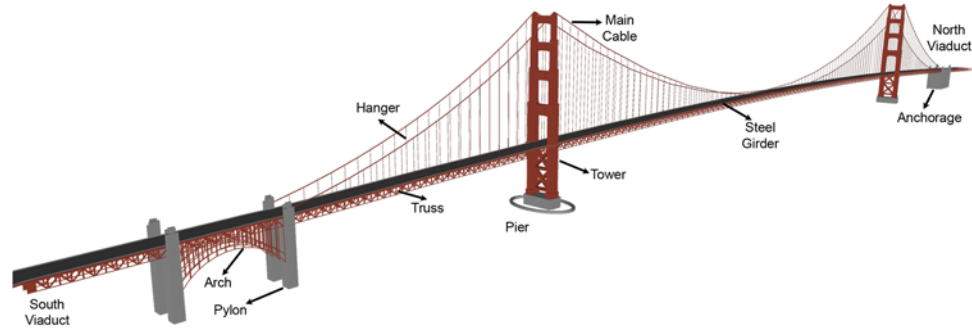


Figure 8. Various parts of the GGB (3D model is taken from Google Earth).

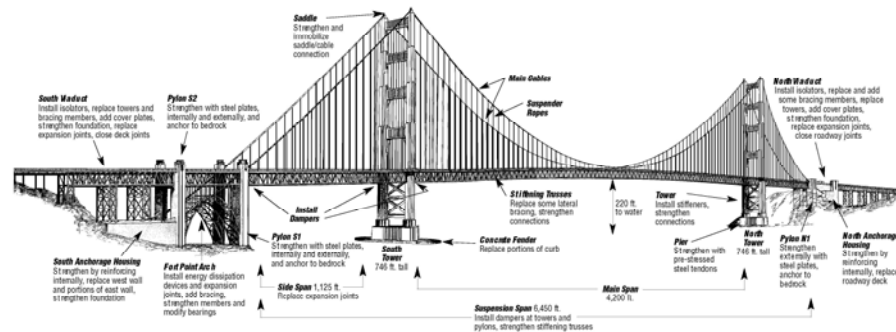


Figure 9. GGB retrofit measures (<http://goldengatebridge.org/projects/retrofit.php>).

Prior Identification Studies

The oldest study on vibration-based identification of the GGB goes back to 1947 when Nishkian measured vertical movement of the bridge deck during its operation [19]. Later, Vincent carried out similar measurements using more accurate sensors and compared real-life data and model prediction [20], [21]. He used data recorded in a 15 years period by suspended mass accelerometers and identified first asymmetric, first and second symmetric vertical natural frequencies of the deck as 0.095, 0.125, and 0.158 Hz, respectively. He also reported torsional frequency of deck as 0.20 Hz. The rate of studies (not specifically on system identification topic) on this bridge got accelerated in 90's. Tanaka and Davenport [22] re-examined data used by Vincent [20]. They also experimentally tested a taut-strip model in laboratory under wind turbulence and concluded that at low speed wind first asymmetric mode is the dominant one. Abdel-Ghaffar and Scanlan [15], [16] conducted extensive experimental investigations on the bridge to determine natural frequencies, mode shapes, and damping ratios from ambient data. They used spectral peak picking for natural frequency identification, cross-spectrum analysis for mode shape identification, and half-power bandwidth method for damping ratio estimation. They could identify 20 vertical, 18 torsional, 33 lateral, and 20 longitudinal modes of the suspended span in the frequency range of 0 to 1.5 Hz and 20 longitudinal, 15 torsional, and 11 lateral modes of the towers in the frequency range of 0 to 5 Hz.

Pakzad et al. [23] designed and implemented a scalable wireless sensor network and used it for modal identification of GGB from ambient data collected in summer of 2006. They limited their analysis to modes below 5 Hz. As they used wireless sensor network, they could measure vibration using various instrumentation layouts. Through their study, it is clearly understood that

for such large and flexible structure, identification could be subjected to spatial aliasing³ if the number of measurement nodes is small. Based on their results, first vertical, transverse and torsional modes are at 0.106, 0.228, and 0.230 Hz, respectively, where all these modes are asymmetric [24]. This valuable dataset were later used several times for verification and validation of some identification methods and frameworks. For example, Pakzad et al. [25] verified the performance of the distributed modal identification approach through this dataset. Chang and Pakzad [26] verified their modified Natural Excitation Technique (NExT) using same data. Also in 2014, same data was analyzed by Matarazzo and Pakzad [27] through pseudo mobile sensing data⁴ and they used structural identification using expectation maximization (STRIDE) [28] to identify modal properties of the GGB from ambient data. Their results were as accurate as those identified before [24].

In 2012, Çelebi [18] carried out an extensive study on the GGB. He analyzed data recorded during three weak earthquakes (Bolinás 1999, Yountville 2000, and Alum Rock 2007). He employed spectral analysis [29] for output-only and Auto-Regressive with eXogenous input (ARX) [30] for input-output identification purposes. This study is the first one in which modal characteristics are identified from earthquake data. He filtered out frequencies below 0.05 and above 50 Hz. While this study provides us with precious information, it suffers from some definiteness. It is done before 2014 South Napa earthquake. Amplitude spectra are not a reliable method for identification of earthquake data, while input-output ARX technique suffers from the fact that it cannot consider multiple support excitations. Even under uniform excitation assumption, any input-output identification technique gives us modal characteristics between only input and output locations. So, any flexibility provided by boundaries, like soil, is excluded.

Recorded Earthquake Data

Following the 1989 Loma Prieta earthquake, it was recommended to instrument large bridges in the California [31]. The seismic instrumentation was planned in 1992 by the CSMIP and the GGB, Highway and Transportation District in cooperation with an appointed seismic instrumentation advisory board [3]. In 1995 (prior to retrofit), 72 accelerometers (15 on the north viaduct and anchorage housing; 33 on the suspension bridge; 22 on the south viaduct and anchorage housing and Fort Arch; 3 at the south free-field; 3 at a downhole under the south viaduct) and 4 relative displacement sensors were installed [32]. After completion of the Phase 1 of the retrofit, 18 sensors were installed on the north viaduct and anchorage housing and a geotechnical array with 6 sensors was installed near the north viaduct. Finally, 22 more sensors were added after completion of the Phase 2. The current locations⁵ of the sensors on the suspension bridge are shown in **Figure 10**.

³ This is not explicit conclusion of that study, and is concluded by this paper's authors based on the results presented in [23]. Also, the term spatial aliasing is not a common term in signal processing.

⁴ Pseudo mobile sensing data is the data without actually implementing mobile sensor network and is extracted directly from a fixed sensor data matrix provide that the paths of the mobile sensors are known.

⁵ Last update: 10/31/2016

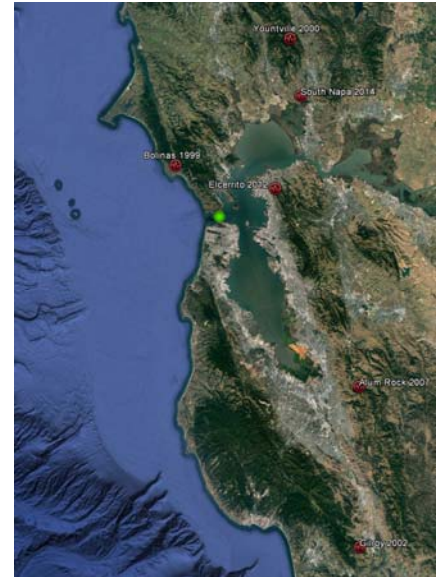
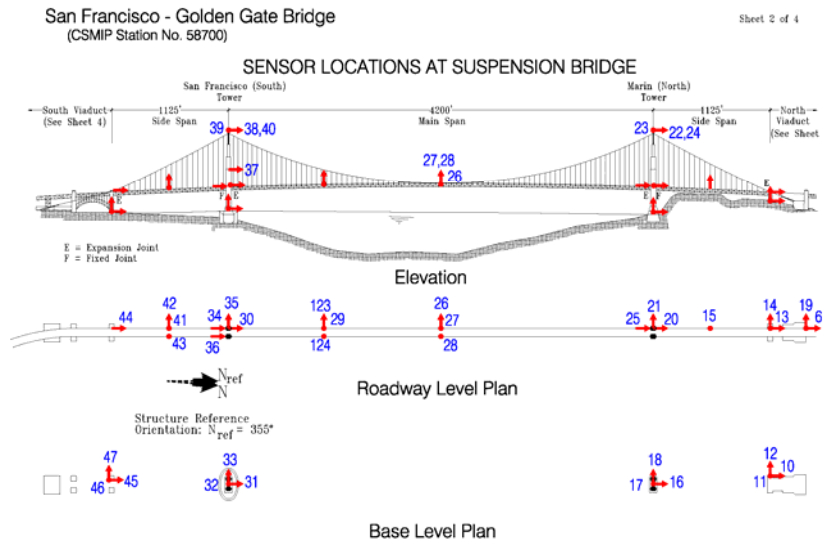


Figure 10. Locations of strong-motion sensors on the suspension span of the Golden Gate Bridge (www.strongmotioncenter.org, last accessed 1/1/2017).

Figure 11. Geographical distribution of earthquake centers around the Golden Gate Bridge.

Several earthquakes have been recorded by the GGB instrumentation system by today (see, **Table 2** and **Figure 11** for these earthquakes’ properties and geographical distribution around the GGB); however, a few of them are publicly available through the CESMD. As it will be discussed in the next section, earthquake data up to 2007 are already studied by Çelebi [18]. Herein, we only study the latest earthquake, i.e., 2014 South Napa earthquake. Note that data of Elcerrito earthquake is not available in CESMD. As it can be seen in **Table 2**, Peak Structural Acceleration (PSA) is highest in the South Napa earthquake in comparison with other prior earthquakes.

Table 2. Earthquakes recorded by GGB instrumentation system (Last update: 1/1/2017)

Earthquake	Date/Time UTC	Magnitude	Depth (km)	Epicentral Dist. (km)	PGA (g)	PSA (g)
Bolinas	8-17-1999/1:06	4.5 (Mw)	7.0	20.6	0.020	0.112
Yountville	9-3-2000/8:36	5.0 (Mw)	5.0	62.1	0.009	0.039
Gilroy	5-13-2002/05:00	4.9 (Mw)	7.6	122.5	0.010	0.071
Alum Rock	10-30-2007/03:04	5.4 (Mw)	9.2	75.5	0.012	0.036
Elcerrito	3/5/2012/13:33	4.0 (ML)	9.2	19.6	0.016	0.084
South Napa	8-24-2014/10:30	6.0 (Mw)	11.3	46.7	0.012	0.181

Due to very sparse instrumentation (**Figure 10**) it is crucial to limit frequency band to prevent phenomenon we can call it spatial aliasing. As it was described in the previous section, due to the size and flexibility of the system, there are many modes in the original frequency range of data (0-50 Hz). So, using such sparse instrumentation it would almost impossible to distinguish modes. As an example, first 8 mode shapes of the suspension part which are identified from ambient signals through dense instrumentation by Abdel-Ghaffar [15] are redrawn in **Figure 12**. On this figure, available sensors deployed through CSMIP which could measure bridge response during 2014 South Napa earthquake are shown by red circles. In the

best scenario, we could be only able to identify mode shapes as displayed by red solid lines. As it can be seen from this figure, there is no meaningful difference between first symmetric and fourth asymmetric modes shapes through available sensors, for example. Or, AS3 and S4 mode shapes are very similar to each other. Note that these modes are all lowest modes and the similarity of mode shapes will highly increase for higher modes. As Blind Modal Identification (BMID) method [33]–[36], which will be used later to identify modal properties from output signals, relies heavily on linear independency of mode shapes, we have to eliminate higher modes from our analysis. Therefore, we apply a low-pass filter to only keep a few fundamental modes. As studied by Pakzad and Fenves [24], there are, for example, 15 vertical modes below 1 Hz, so we filter out frequencies higher than this value. Also, due to low frequency errors observed in the signals, frequencies below 0.05 Hz are also filtered out through high-pass filter. Recorded acceleration signals on the suspension part are shown in **Figure 13** in which all records are shown with same scale. Also, first 20 seconds of the signals are not shown, because there is no significant motion. As this figure shows response of the deck in the vertical direction and longitudinal and transverse vibration of the towers have highest level of motion.

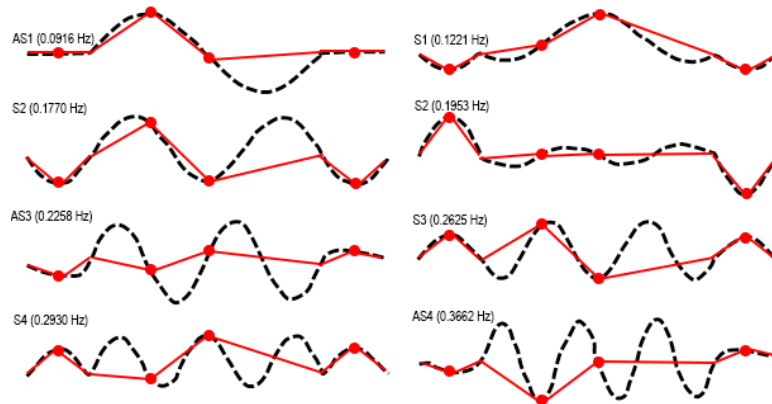


Figure 12. Mode shapes identified from ambient testing [15] (black curves), permanent sensors (red circles), and identifiable mode shapes (red lines).

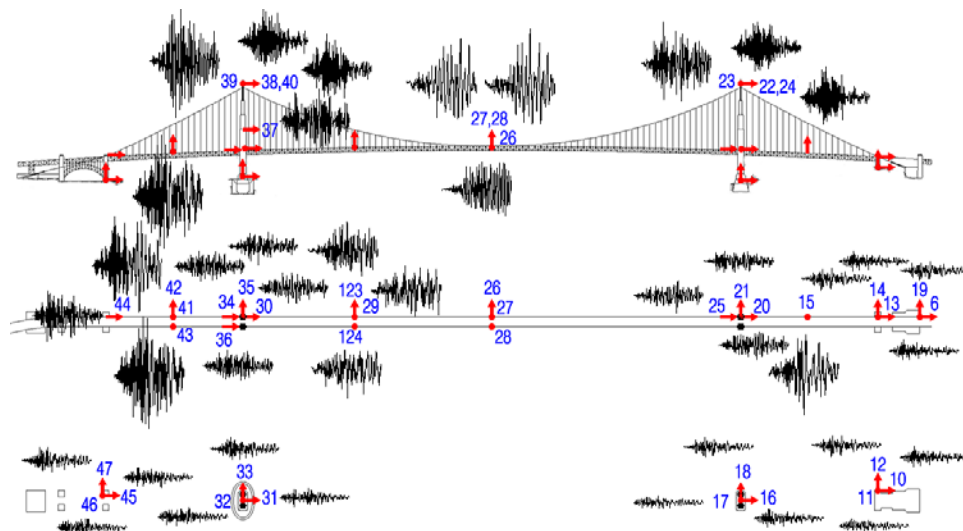


Figure 13. Recorded acceleration signals on the suspension part of the GGB.

To make sure that the frequency range of under study contains most energy content of the signals, maximum displacement responses after filtering are normalized with original values and shown in **Figure 14**. As it can be seen, this ratio is higher than 0.8 for most of the channels. Specifically, for those channels recorded on suspension part (foundation, deck, and tower levels), this value is close to 0.9. Note that those few cases with value less than 0.8 are related to low frequency errors which are removed through high-pass filtering.

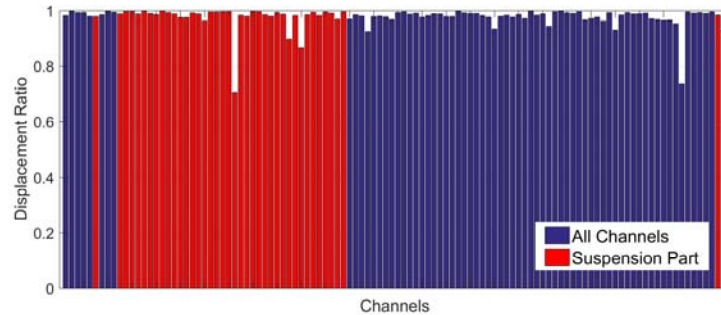


Figure 14. Ratio of after filtering maximum displacement values to the original values.

As will be discussed later, material nonlinearity will not be included in the model. Herein, we carried out a visual observation on observed dominant frequencies to make sure that there is no significant nonlinearity in the system. To do so, we present time-frequency representation [37] of a few signals. As a first example, time-frequency representation of CH27+CH28 (vertical movement of the mid-span) is presented in subplot (b) of **Figure 15**(left). Acceleration time history of the signal is also shown in subplot (a). As it can be seen, a very dominant frequency at 0.3067 Hz with a minor contribution from 0.6733 Hz is observed in this figure. High level of energy of the 0.3067 Hz component may mask contribution of other components. To resolve this issue, time history is scaled by its instantaneous amplitude as described in [38]. This figure is shown in subplot (c) of **Figure 15**(left). Interestingly, two other frequencies appear now. During first ~20 seconds, bridge is vibrating in its fundamental mode ~0.1333 Hz due to ambient excitations. After arriving seismic waves, higher modes at 0.3067, 0.6733, and 0.8867 Hz get excited, while mode at 0.3067 persistently exists by the end of the record.

Figure 15(right) presents same graphs for deck’s torsional vibration estimated through CH27-CH28. Again, through time-frequency representation and with help of amplitude scaling, it is possible to observe contribution of different modes at different time instants. At the very beginning, a mode at 0.3333 Hz is dominant, then mode at 0.2333 Hz gets dominated for 20 seconds until the arrival of severe seismic waves. After a short period of time in which a higher frequency of 0.8133 Hz is present, most part of the signal is affected by a mode at 0.5733 Hz.

Frequencies named at two paragraphs above can be labeled according to the prior studies and frequency closeness. These labels are shown in **Table 3** and are deduced from Abdel-Ghaffar’s experimental study [15].

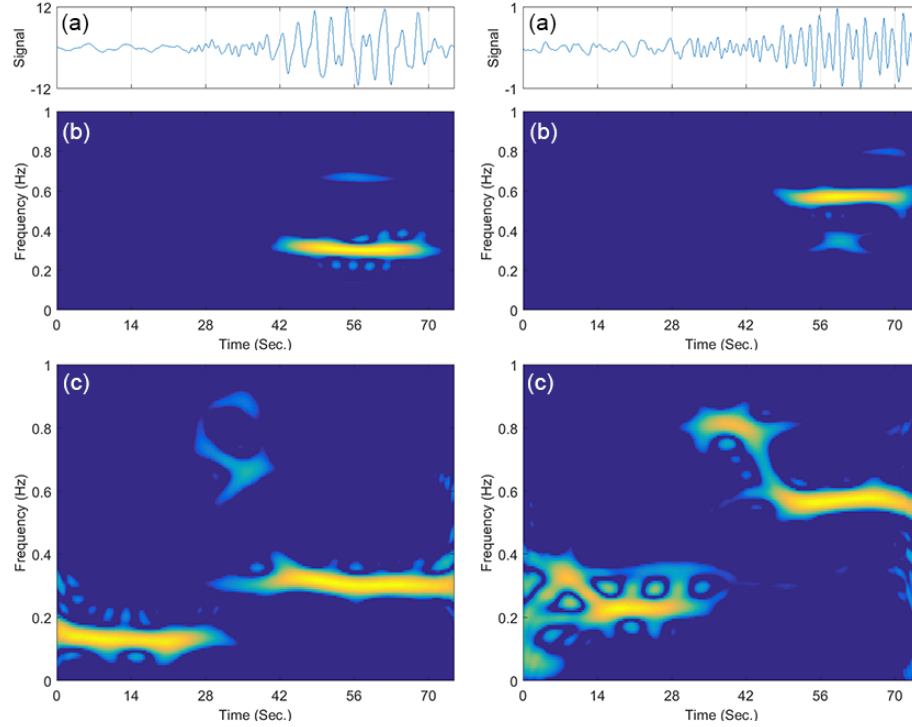


Figure 15. Time and time-frequency representation of CH27+CH28 (left) and CH27-CH28 (right).

Table 3. Labels of the modes observed in **Figure 15** [15].

Frequency (Hz)	0.1333	0.2333	0.3067	0.3333	0.6733	0.5733	0.8133	0.8867
Mode	VS1	TS1	VS4	TS2	VS7	TS4	TS6	VS9

V: Vertical; T: Torsional; S: Symmetric

One of the main objectives of this study is to investigate any spatial variability in bridge's FIMs. This bridge has sensors on its foundation level, so foundation response could be FIMs provided that there is no inertial soil-structure interaction effect. Let's assume that there is no inertial SSI effects and assume foundation response as FIM. In the absence of any spatial variability, input excitation experienced by the ridge at its all piers must be similar with only possible phase delay effect. To check the similarity between two signals, say $s_i[n]$ and $s_j[n]$, sample cross-covariance index is employed here [29], which is calculated as

$$c_{ij}[k] = \frac{1}{N} \sum_{n=0}^{N-k} (s_i[n] - \bar{s}_i) (s_j[n+k] - \bar{s}_j) \quad (8)$$

where $k = 0, 1, \dots, N - 1$, and N is number of time samples. \bar{s}_i and \bar{s}_j indicate the mean of two signals. It is also possible to calculate $c_{ij}[k]$ for negative lags, which are indeed obtained by changing the i and j sub-indices at the summation above. $c_{ij}[k]$ is usually normalized with the square-root of $c_{ii}[0]$ and $c_{jj}[0]$ to keep the value of covariance between -1 and 1 . This normalized value is termed the *cross-correlation* in time series analysis. A cross-correlation

equal to -1 or $+1$ denotes two signals are identical except with a time lag, whereas a cross-correlation close to zero means that they are not similar.

Figure 16 shows $c_{ij}[k]$ versus time lags for $i, j = \text{CH47, CH33, CH 18, and CH12}$, which are four transverse channels at four piers. Peak value of the cross-correlation is depicted by using a vertical dashed line and the absolute value of time lag corresponding to these peaks are written on each subplot. Several significant observations are deduced from this figure. First, all peak values are at negative time lags showing that if there is wave propagation, it is from North (Marin) to South (San Francisco) direction. Second, the peak level of correlation is very low between all pairs of channels, showing there is significant incoherency [39]. Third, assuming plane waves with similar incident angle, the average value of the surface apparent wave velocity obtained by dividing horizontal distance between each two channels by these time lags is around 4400 m/s.

Similar figures for Longitudinal and Vertical channels are produced but not shown for the sake of space. For Longitudinal direction, channels 45, 31, 16, and 10, and for the Vertical direction channels 46, 32, 17, and 11 are used. It was observed that similar comments can be made on these directions too. If we calculate the surface apparent wave velocity corresponding to the observed delays, it could be around 6000 and 7000 m/s for longitudinal and vertical directions, respectively. It is noteworthy to mention that estimation of the delay through cross-correlation gives us an average of the group delay if the medium of the wave propagation is dispersive.

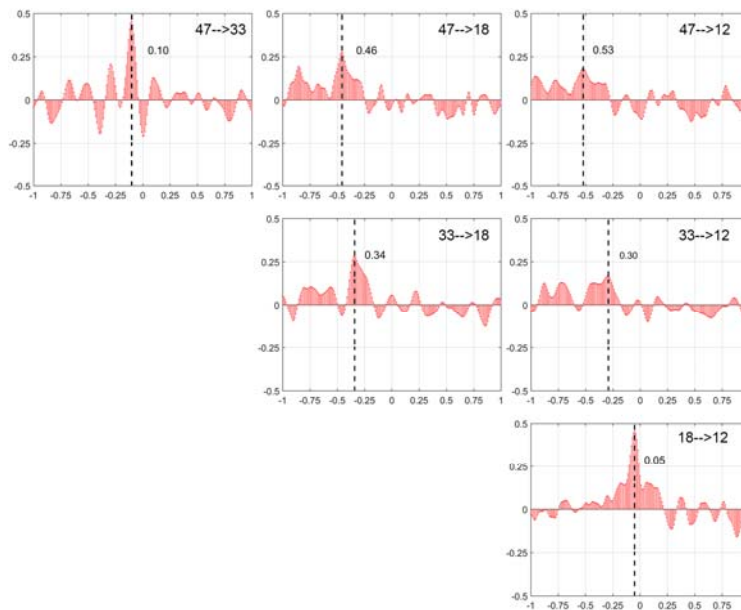


Figure 16. Cross-correlation among acceleration channels on the foundation level in Transverse direction. Horizontal axes are time lags (in seconds) and vertical axes are cross-correlation.

Numerical Modeling

Up to the knowledge of the authors, first numerical study on the GGB was carried out by Baron et al. [40] in 1976. They created linear 2D (with 278 nodes) and 3D (with 120 nodes) models to investigate dynamic behavior of the bridge in longitudinal-vertical and transverse-

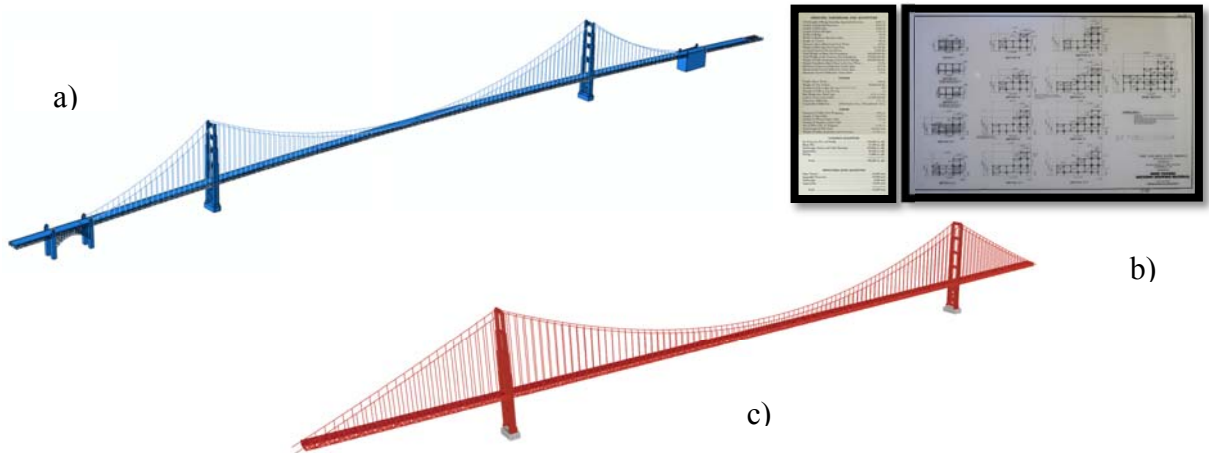
torsional directions, respectively. Both models were fixed at the towers' bases. Static, eigenvalue, and time history analyses were carried out in this study. The model was excited under both uniform and multiple support excitations. However, only wave passage effect was considered. Also, a Rayleigh damping matrix with mass and stiffness proportional factors of 0.04805 and 0.0065 were used.

Abdel-Ghaffar [41] was one of pioneering researchers who studied dynamic response of suspension bridges. He employed frequency-domain random vibration approach to analyze GGB under multi-support excitations. Both vertical (induced by vertical and longitudinal excitations) [42], [43] and lateral [44], [45] earthquake-induced response of the GGB under multiple support excitations were studied. 2D linearized Finite Element models developed by Abdel-Ghaffar which were later used in several studies [15], [16] consisted of 283 beam elements with 193 movable nodes, resulting in a system with 1146 degrees of freedom. Axial tension effects of the cables were included by the addition of a geometric stiffness matrix to the elastic stiffness matrix [46]. In the most fundamental symmetric and ten asymmetric vertical, torsional, and transverse modes, there was a very good agreement between numerical and experimental mode shapes and natural frequencies. He also showed that his simpler 2D models work as accurately as 3D model developed by Baron et al. [40].

As mentioned earlier, after 1989 Loma Prieta earthquake, a series of studies for the purpose of seismic evaluation and possible retrofit were initiated. The district engaged T. Y. Lin International (TYLI) to perform these evaluation studies [47], while sub-consultants Imbsen & Associates, Inc. (IAI) and Geospectra, Inc. (GI) were also engaged. The 3D model of the main bridge used in that evaluation had been originally developed for TYLI's Transit Feasibility study [48]. This model was composed of 9933 frame elements connecting 4775 nodes, which was reduced by using a super-element formulation such that the total number of active degrees of freedom was around 4000 [14]. Similar to Abdel-Ghaffar's studies, dynamic loads and responses was regarded as disturbances to the dead-load configuration, so the analysis problem was linearized with response respect to the dead-load state of the structure. Also, geometrical nonlinearity was considered by using geometric stiffness matrices. This global model went under several analyses including linearized time history analysis under multiple-support earthquake excitation. In addition to this global model, several more detailed linear and nonlinear analyses were carried out by local modes, e.g., tower-to-pier connection. Results of these studies were later published in several papers and reports [17], [49]–[54]. In a very recent work, Game et al. [55] created a 3D model of the GGB in Strand7 [56]. While they kindly shared their model with us, the model was not accurate in geometry and details.

In the present study, a new 3D model is created. To create such model with highest accuracy in geometry, the geometry was taken from Google Earth which was already shown in **Figure 8**. This model was taken to the ABAQUS [57] to convert faces and lines to a 3D model with solid elements. This model is shown in **Figure 17(a)**. A model with solid elements is computationally very expensive and cannot be used in output-only identification framework described in the previous section. Hence, solid elements were replaced with structural elements in SAP2000 [58], which is shown in **Figure 17(c)**. To create this model, publicly available details [13] on this bridge, sample of which is shown in **Figure 17(b)**, were taken into account along with all quantitative and qualitative description found in other researcher's studies reviewed in prior sections. Finally, to take advantage of parallel processing, this SAP2000 model was transformed to OpenSEES [59] using a Matlab [6] interface developed by the authors, which

uses SAP Application Programming Interface (API) to communicate to SAP2000. This Matlab code enables us to repeat the process for any other structure. The final OpenSEES model is



shown in **Figure 18**.

Figure 17. (a) Abaqus model, (b) samples of available structural details, and (c) SAP2000 model.

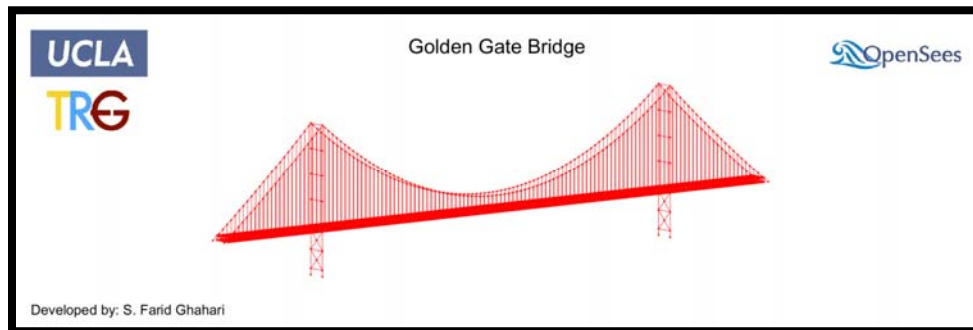


Figure 18. OpenSEES model of the GGB.

The OpenSEES model is composed of more than 20000 Degrees-Of-Freedom (DOFs) with more than 8000 frame elements and 2000 area elements. In the original SAP2000 model, cables and hangers were modeled as cable elements and main cables' geometry was determined iteratively such that after imposing dead load they have internal stress and maximum sag as reported by Abdel-Ghaffar [15]. In the OpenSEES, cables and hangers are modeled using Co-rotational truss element with material which can accept initial stress. While there is no material nonlinearity (except zero compression in cables and hangers) in the model, geometrical nonlinearity was considered, because it is crucial for suspension bridges.

Identifiability

The first step in any identification is to figure out possible sources of uncertainties and identifiability of these uncertainties. As we did not have access to the actual details of the GGB and also this bridge experiences several retrofit stages during its life as reviewed in prior sections, almost all material properties are uncertain. In addition, all connections (like spans'

connections to the towers) and boundaries (like soil-abutment and soil-foundation systems) are modeled by appropriate linear springs with expected values which must be updated through identification process. Also, parameters of Rayleigh damping (the best possible strategy for damping modeling right now) are considered as other potential updating parameters.

In total, there are 66 parameters which are potential candidates for the updating along with FIMs. However, it is not needed/possible to consider all of these parameters in the identification process. Through two sifting steps, the number of updating parameters is much reduced as follows. In the first step, it was identified which parameters have indeed value and which are free or fixed. For example, according to the structural drawings and prior studies, towers do not have relative translation with respect to the main and side spans, so we fixed these connections and excluded them from identification process. Assuming non-fixed connections makes the modal properties of the model deviate from what reported in previous studies. While it is expected not to have significant inertial SSI effects (based on this fact we choose GGB to be able to validate FIMs, indeed), we considered translational and rotational springs of soil-foundation systems as unknowns. However, values of these springs' stiffnesses must be very low to make these springs effective, which are not physically meaningful with respect to the GGB's properties. So, we fixed them too. We also excluded initial tension in cables and hangers, because they have been already considered by applying gravity loads. Based on these facts, 28 parameters out of initial 66 parameters can be potential updating parameters, which are listed in **Table 4**. However, all of these parameters might not be identifiable through available instrumentation layout. To specify identifiability of these parameters, which is second sifting step, we carried out sensitivity analysis to calculate total information for each parameter θ_i as [60]

$$I_i = \sum_{j=1}^m \left(\frac{\partial y_j}{\partial \theta_i} \right)^2 \quad \text{for } i = 1 \dots 28 \quad 9)$$

where $\partial y_j / \partial \theta_i$ is the sensitivity of response at j -th channel with respect to the θ_i and m is the number of all recorded channels. We perturbed θ_i around its nominal value and used Finite Difference to calculate $\partial y_j / \partial \theta_i$. **Figure 19(a)** shows information entropy for all these 28 parameters. Assuming a threshold of 1, for example, 7 parameters are the most informative parameters. This figure shows that from this model and instrumentation layout, it is not possible to infer any reliable information about abutment's springs, mainly because it is a very flexible bridge.

Even, not all of 7 parameters can be uniquely identified. By looking at mutual information among parameters shown in **Figure 19(b)**, it is seen that some parameters are highly correlated with each other. For example, Modulus of elasticity of Chords is correlated with modulus of elasticity of diagonal Bars. So, we fix one (diagonal Bar's) of them and consider the other one as updating parameter (Chord's). Also, because Hanger's and deck's modules of elasticity are also highly correlated with diagonal bar's modules of elasticity, we also fix them.

Finally, we have 4 important parameters (Tower's, Cable's, Chord's, and Bottom Bracing's modules of elasticity) which are identifiable through the present instrumentation layout. While damping parameters are not very informative in comparison with respect to others, we consider them too, because they do not have any correlation with others. So, we carry out the identification with 6 unknown parameters along with 6 time-series of FIMs (3 components at

each pier). We assume same FIMs in south and north abutments as south and north piers, respectively.

Table 4. Candidate parameters after first sifting step.

No.	Element	Parameter
1	Bottom Bracing	Elastic Modules
2	Cable	Elastic Modules
3	Chord	Elastic Modules
4	Deck	Elastic Modules
5	Diagonal Bar	Elastic Modules
6	Floor Beam	Elastic Modules
7	Hanger	Elastic Modules
8	Kneebrace	Elastic Modules
9	Top Bracing	Elastic Modules
10	Tower	Elastic Modules
11	Track Girder	Elastic Modules
12	Transverse Strut	Elastic Modules
13	Vertical Rod	Elastic Modules
14	Vertical Bar	Elastic Modules
15	South Tower-South Side Span	Spring Stiffness, M2
16	North Tower-North Side Span	Spring Stiffness, M2
17	South Abutment	Spring Stiffness, P
18	South Abutment	Spring Stiffness, V2
19	South Abutment	Spring Stiffness, V3
20	South Abutment	Spring Stiffness, T
21	South Abutment	Spring Stiffness, M2
22	North Abutment	Spring Stiffness, P
23	North Abutment	Spring Stiffness, V2
24	North Abutment	Spring Stiffness, V3
25	North Abutment	Spring Stiffness, T
26	North Abutment	Spring Stiffness, M2
27	Damping	Alpha
28	Damping	beta

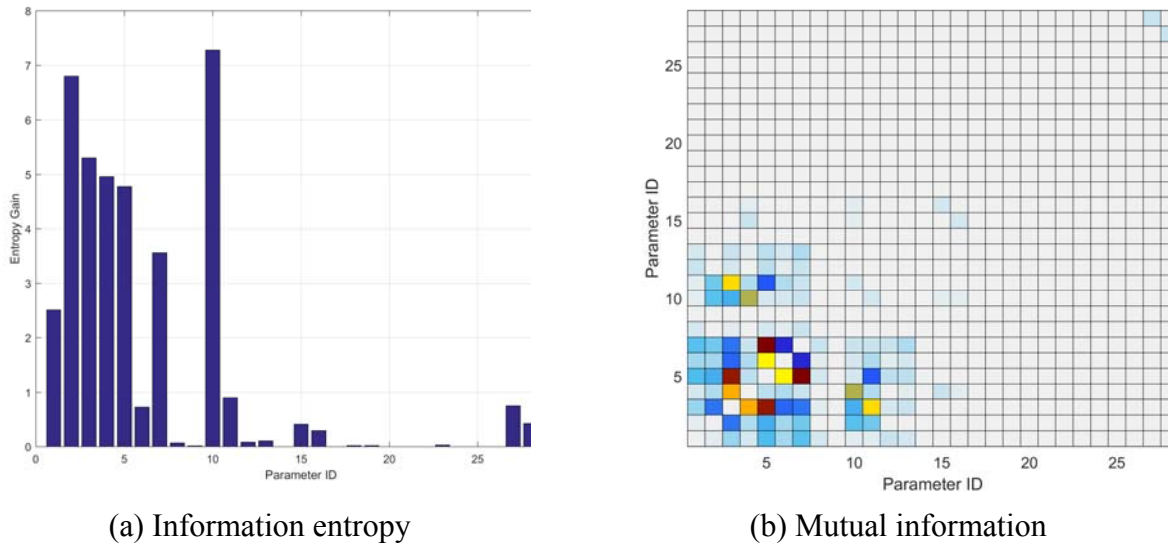


Figure 19. Identifiability analysis. (a) information entropy for each parameter, (b) mutual information among parameters, and (left) list of parameters.

Identification Results

Verification: Simulation Data

Before applying the proposed identification method on the real-life data, it is crucial to verify it through simulated data. The proposed method is able to work for a wide range of applications from linear to nonlinear or input-output to output-only cases. As an initial test, we used it for input-output identification. Such input-output identification is quite useful in real world, because one way to consider soil-structure interaction effects is to modify input motions to include feedback inertia effect. In other words, it is possible to exclude compliance beyond a location by imposing prescribed motion at that location. For example, Shirkhande and Gupta [61] followed same approach to estimate response of the GGB using a fixed-base model. In addition, even complexity of the output-only identification could decrease if an input-output identification using foundation-level measurement carried out first to estimate superstructure’s parameters while soil-foundation parameters. Of course this approach is only applicable if there is measurement on the foundation level.

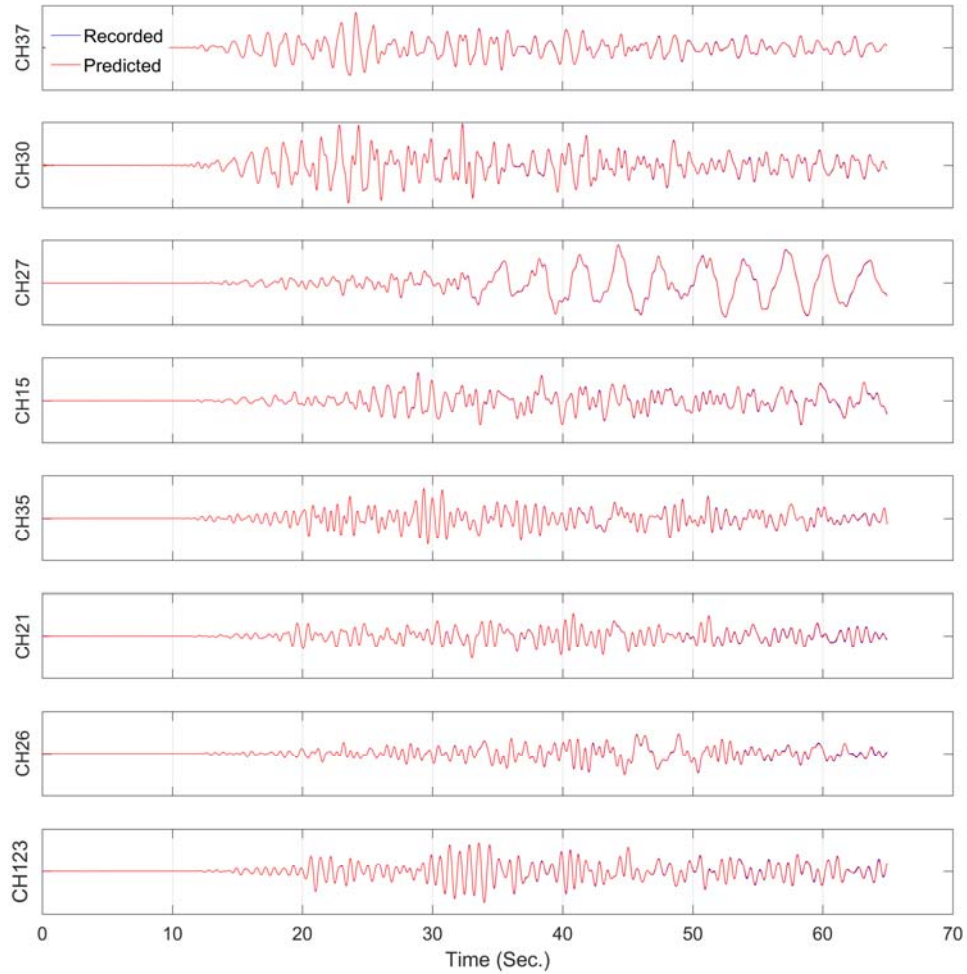


Figure 20. Comparison between recorded (simulated) and predicted acceleration responses at select channels.

We applied this input-output identification on the simulated data of the GGB. **Figure 20** shows comparison between recorded (synthetically simulated) and predicted (at the last iteration of the last updating step) responses at some selected channels. As seen, prediction is perfect. While we assumed 50% initial error in all 6 parameters, final results show 0.03%, 0.04%, 0.23%, 1.59%, 2.38%, and 13.76% error at the end of updating process. As expected, damping parameters are not identified as accurate as others in which stiffness proportional factor is more erroneous, which is in agreement with **Figure 19(a)**.

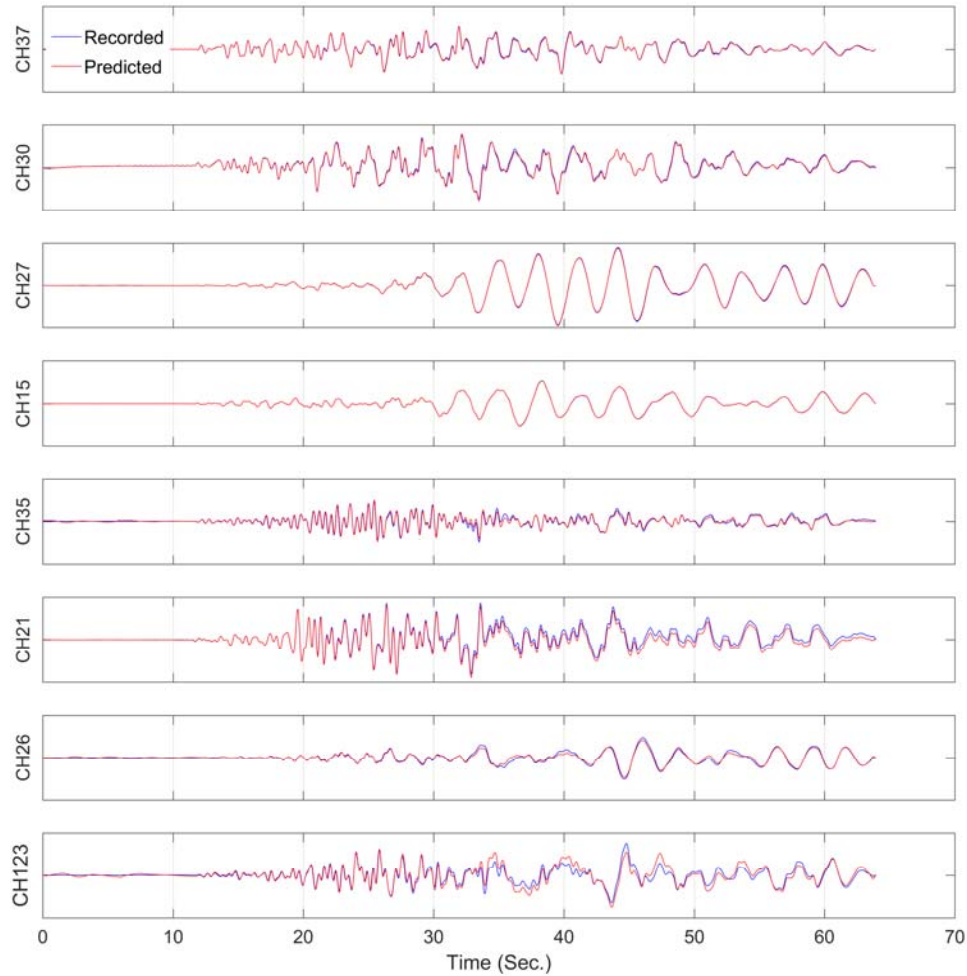


Figure 21. Comparison between recorded (simulated) and predicted acceleration responses at select channels.

While it is possible to use information obtained in the input-output identification step to reduce parameters uncertainty in the output-only identification, we do not use it, because response of the foundations/abutment might not be recorded at all piers in real-life. Therefore, we carry out output-only identification while all 6 parameters along with FIMs are unknown. Assuming an initial error of 20% we obtained 4.28%, 0.25%, 0.56%, 23.94%, 6.78%, and 3.25% for Towers', Cables', Chord's, Braces' modules of elasticity, and mass and stiffness proportional damping coefficients, respectively. While all results are acceptable and expected, identification algorithm was not successful to find modules of elasticity of bottom bracing. Comparison between recorded and predicted responses at some selected channels is shown in **Figure 21**⁶. As seen, while one of parameters is not identified accurately, predicted responses are very close to the recorded ones.

Finally, the most important identification results are FIMs. The identified FIM in the transverse direction on the South pier is shown in **Figure 22** along with its exact counterpart. As this figure shows, the input motion is identified with a very good accuracy especially in time

⁶ We used different damping values in output-only simulation, so response signals are not identical to Figure 20.

windows with high levels of excitation. The other FIMs are also identified with the same level of accuracy, which are not shown here for brevity.

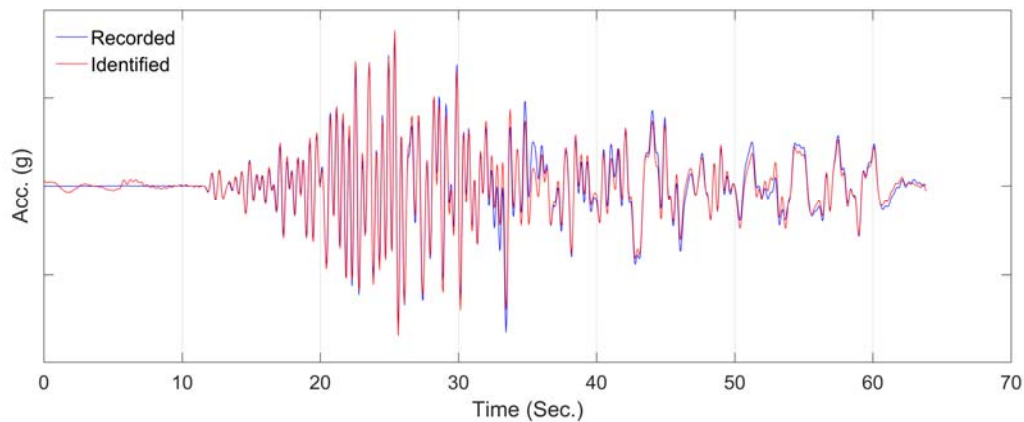


Figure 22. Comparison between exact and identified FIM in transverse direction on the South pier.

Validation: Real-Life Data

Herein, we replace simulated signals with their real-life recorded counterparts and carry out input-output and output-only identification as carried out in the previous section. **Figure 23** compares recorded and predicted acceleration responses at some selected channels in the input-output identification. As expected, results are not as good as synthetic data. However, the level of accuracy varies among channels. Predicted responses at channels 37, 30, 35, and 21 are very close to the real-life data. All these channels are on the towers or very close to the towers. Response prediction at the Channel 15 is acceptable, although there are some high frequency components which are not captured in the prediction. The major discrepancies are observed at channels 26, 27, and 123. All these channels are on the main span. Several reasons could be possible source of such inconsistencies. First off, we did not have access to all details of the bridge, so there could be some modeling uncertainties in addition to parameter uncertainties. Secondly, responses at these channels are highly affected by the other co-existing excitations like due to wind and moving vehicles, which are not considered here. Finally, we modeled damping through the Rayleigh method, which might not be able to accurately model damping for all modes. This could be significant for the main-span channels, because many modes are contributing to these signals, while channels on the tower mostly contain only a few fundamental modes of the system.

While we considered wide boundaries for the updating parameters, all modules of elasticities are identified around $2 \times 10^{11} \text{ N/m}^2$ except those of the bottom bracings, which are around $2.5 \times 10^{11} \text{ N/m}^2$. This indicates that perhaps the dimensions of bottom bracing elements were underestimated in the model. Identified Rayleigh damping parameters are both around 0.1.

Predicted responses and one of identified FIMs obtained in output-only identification are shown in **Figure 24** and **Figure 25**, respectively. As seen, the similarity level between recorded and predicted responses is close to what we observed for the input-output case (**Figure 23**) while here FIMs are also identified. One of the identified FIMs is shown in **Figure 25**. Assuming that what is recorded on the foundation is true FIM (inertial SSI is negligible), these two signals are

quite similar, but the amplitude of the identified FIM is higher than the recorded foundation response. The authors believe that this is because level of input excitation is compromised with overall damping of the system. This issue could be addressed in future by introducing damping more specifically, especially when system is going under nonlinear behavior. In other words, by parametrizing sources of damping, e.g., backbone curves of plastic hinges, relationship there would be no linear relationship between input, damping, and response, so both input and damping could be identified more accurately.

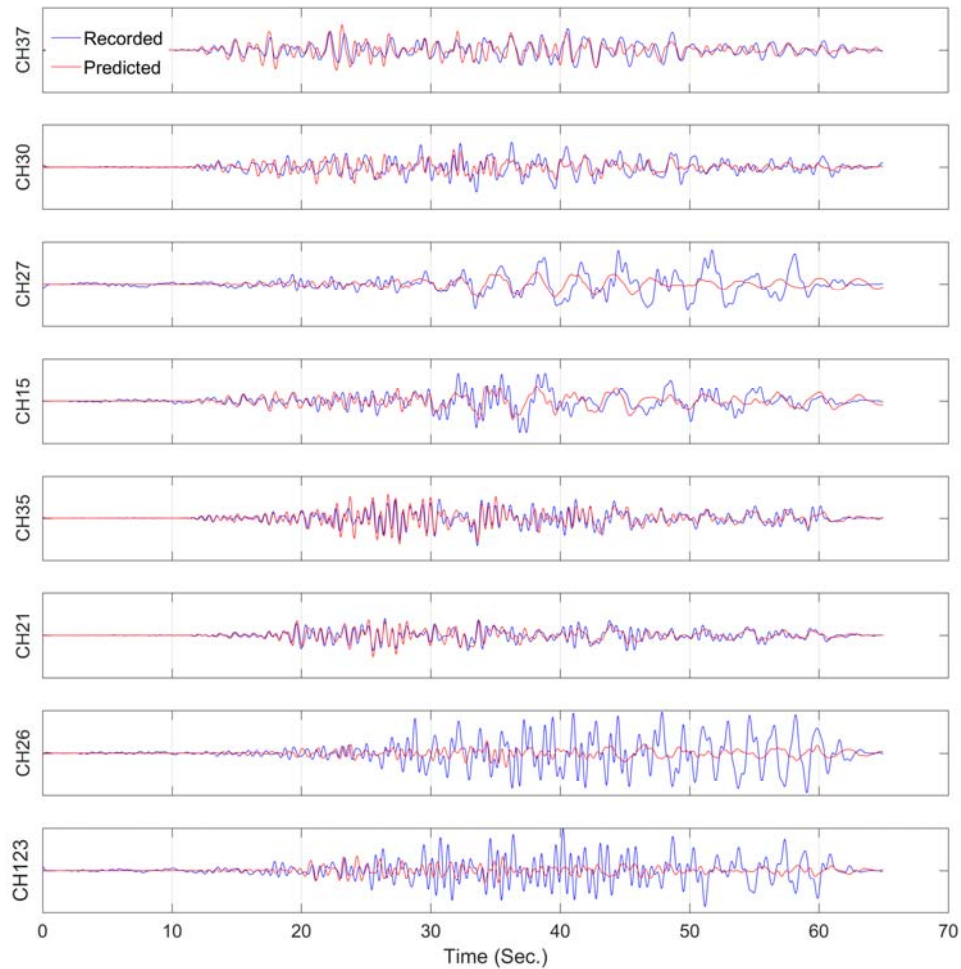


Figure 23. Comparison between recorded and predicted acceleration responses at select channels.

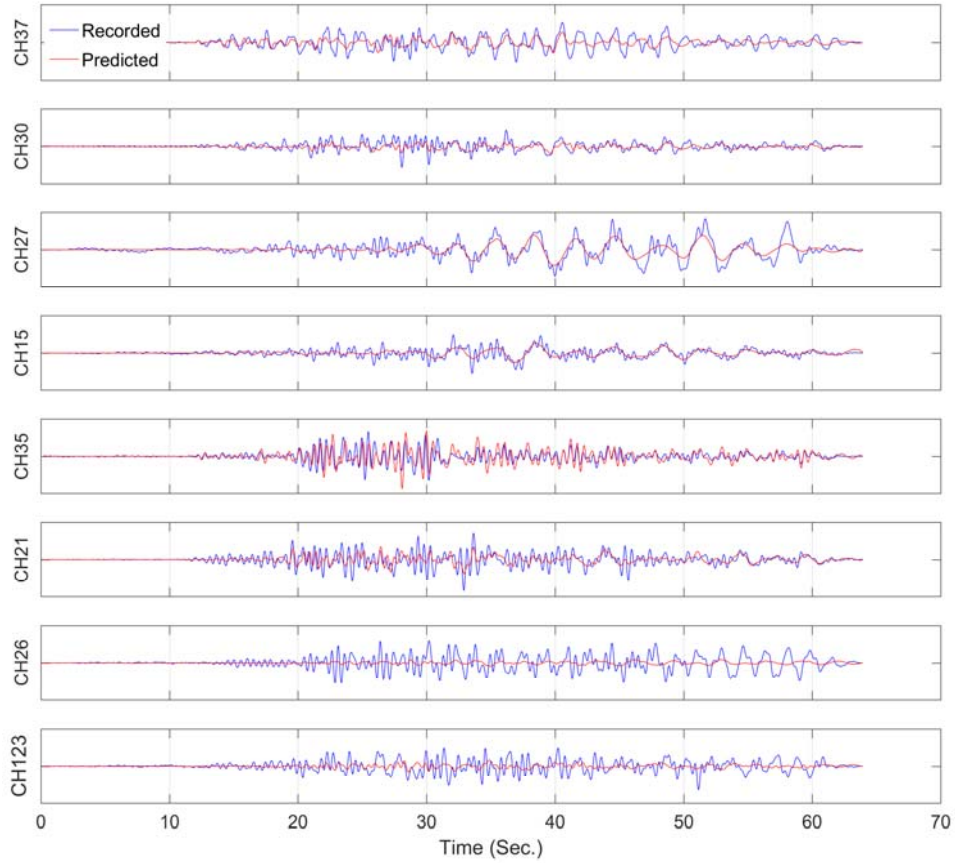


Figure 24. Comparison between recorded and predicted acceleration responses at select channels.

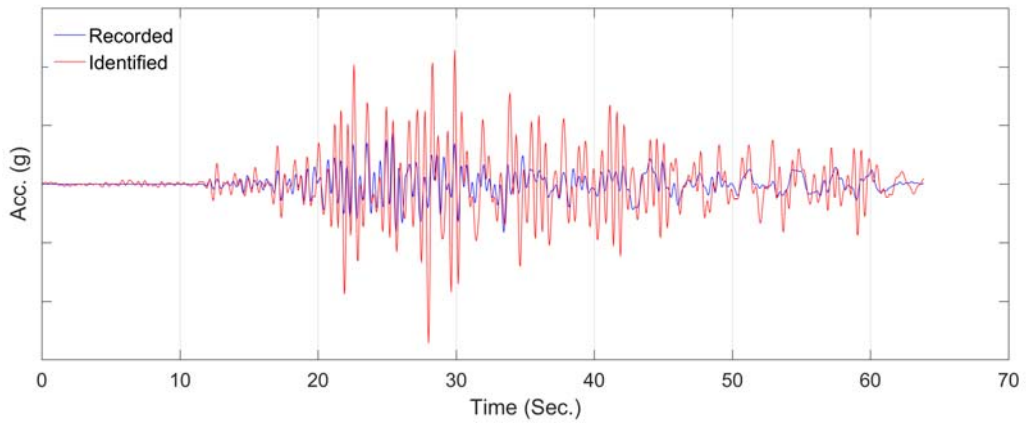


Figure 25. Comparison between recorded foundation response and identified FIM in transverse direction on the South pier.

Conclusions

This study presented a verification and validation study whose objective is to quantify the spatial variability in bridge Foundation Input Motions (FIMs) using data recorded during the 2014 South Napa Earthquake. This aspect comprised the development and verification of two distinct (and new) methods. The first of these was an output-only system identification method that yields time-history estimates of FIMs at all bridge piers from accelerations recorded on the bridge. The second was a blind channel identification method that enables the identification of local site effects at each pier provided that all FIMs are caused by a single excitation source and the kinematic interaction is similar at all piers. The second method was presented in our first phase of study at SMIP16. The applicability of the second method—i.e., the output-only identification method—was tested in the present paper through an extensive study on both simulated and real-life data from the Golden Gate Bridge. The results of this study showed that the proposed framework is able to recover FIMs from sparsely measured responses of a complex bridge. To the best of our knowledge, this is the only study in which multiple FIMs are identified with real-life recordings from a bridge structure.

Acknowledgement

The authors would like to acknowledge Dr. Celebi from USGS, and Prof. Asimaki from Caltech for their valuable comments and help. Also, Dr. D’Auria from UCLA Institute for Digital Research and Education helped us to carry out analyses on UCLA Hoffman cluster, which is appreciated. The work presented in this manuscript was funded, in part, by the California Geological Survey (Contract No. 1014-963) and by the California Department of Transportation (Grant No. 65A0450). Any opinions, findings, conclusions or recommendations expressed in this material are those of the authors and do not necessarily reflect the views of the sponsoring agencies.

References

- [1] A. Zerva and V. Zervas, “Spatial variation of seismic ground motions: An overview,” *Appl. Mech. Rev.*, vol. 55, no. 3, p. 271, 2002.
- [2] E. Taciroglu and S. F. Ghahari, “Identification of spatial variability in bridge foundation input motions: Theoretical basis,” in *Proceedings of SMIP16 Seminar on Utilization of Strong-Motion Data*, 2016.
- [3] A. F. Shakal, C. D. Petersen, A. B. Cramlet, and R. B. Darragh, “CSMIP near-real-time strong motion monitoring system: Rapid data recovery and processing for event response,” in *Proceedings SMIP95 Seminar on Seismological and Engineering Implications of Recent Strong-Motion Data*, Huang, MJ, Ed, 1995.
- [4] S. F. Ghahari, F. Abazarsa, C. Jeong, A. Kurtulus, and E. Taciroglu, “Blind identification of site effects and bedrock motions from surface response signals,” *Soil Dyn. Earthq. Eng.*, 2017 (under review).
- [5] E. Ghahari, S.F., Abazarsa, F., Taciroglu, “Probabilistic Blind Identification of Site Effects from Ground Surface Signals,” *Bull. Earthq. Eng.*, 2017 (under review).
- [6] MATLAB, Online manual—*Components*, vol. 3, no. 7, p. 750, 2004.
- [7] CESMD, “Center for Engineering Strong Motion Data,” 2017. [Online]. Available: <http://strongmotioncenter.org/>. [Accessed: 01-Jan-2017].

- [8] H. Huang, J. N. Yang, and L. Zhou, “Adaptive quadratic sum-squares error with unknown inputs for damage identification of structures,” *Struct. Control Heal. Monit.*, vol. 17, no. 4, pp. 404–426, 2010.
- [9] R. Astroza, H. Ebrahimian, Y. Li, and J. P. Conte, “Bayesian nonlinear structural FE model and seismic input identification for damage assessment of civil structures,” *Mech. Syst. Signal Process.*, vol. 93, pp. 661–687, 2017.
- [10] H. Ebrahimian, R. Astroza, J. P. Conte, and R. A. de Callafon, “Nonlinear finite element model updating for damage identification of civil structures using batch Bayesian estimation,” *Mech. Syst. Signal Process.*, pp. 1–29, 2016.
- [11] S. Haykin, *Kalman Filtering and Neural Networks*, vol. 5, no. 3. 2001.
- [12] S. J. Julier, “New extension of the Kalman filter to nonlinear systems,” in *Proceedings of SPIE*, 1997, pp. 182–193.
- [13] J. B. Strauss and C. E. Paine, *The Golden Gate bridge: report of the chief engineer to the Board of directors of the Golden Gate Bridge and Highway District, California, September, 1937*. Golden Gate Bridge, Highway and Transportation District, 1938.
- [14] M. A. Ketchum and C. Seim, *Golden Gate bridge seismic evaluation*. TY Lin International, 1990.
- [15] A. M. Abdel-Ghaffar and R. H. Scanlan, “Ambient vibration studies of golden gate bridge: I. Suspended structure,” *J. Eng. Mech.*, vol. 111, no. 4, pp. 463–482, 1985.
- [16] A. M. Aabdel-Ghaffar and R. H. Scanlan, “Ambient Vibration Studies of Golden Gate Bridge: II. Pier-Tower Structure,” *J. Eng. Mech.*, vol. 101, no. 4, pp. 483–499, 1985.
- [17] T. J. Ingham, S. Rodriguez, M. N. Nader, F. Taucer, and C. Seim, “Seismic retrofit of the golden gate bridge,” in *Proc., National Seismic Conf. on Bridges and Highways: Progress in Research and Practice*, 1995.
- [18] M. Çelebi, “Golden Gate Bridge response: A study with low-amplitude data from three earthquakes,” *Earthq. Spectra*, vol. 28, no. 2, pp. 487–510, 2012.
- [19] L. H. Nishkian, “Vertical vibration recorders for the Golden Gate Bridge,” *Bull. Seismol. Soc. Am.*, vol. 37, no. 2, pp. 81–88, 1947.
- [20] G. S. Vincent, “Golden Gate bridge vibration studies,” *Trans. Am. Soc. Civ. Eng.*, vol. 127, no. 2, pp. 667–701, 1962.
- [21] G. S. Vincent and M. Labse, “Correlation of predicted and observed suspension bridge behavior,” *Trans. Am. Soc. Civ. Eng.*, vol. 127, no. 2, pp. 646–666, 1962.
- [22] H. Tanaka and A. G. Davenport, “Wind-Induced Response of Golden Gate Bridge,” *J. Eng. Mech.*, vol. 109, no. 1, pp. 296–312, 1983.
- [23] S. N. Pakzad, G. L. Fenves, S. Kim, and D. E. Culler, “Design and Implementation of Scalable Wireless Sensor Network for Structural Monitoring,” *J. Infrastruct. Syst.*, vol. 14, no. 1, pp. 89–101, 2008.
- [24] S. N. Pakzad and G. L. Fenves, “Statistical Analysis of Vibration Modes of a Suspension Bridge Using Spatially Dense Wireless Sensor Network,” *J. Struct. Eng.*, vol. 135, no. 7, pp. 863–872, 2009.
- [25] S. N. Pakzad, G. V. Rocha, and B. Yu, “Distributed modal identification using restricted auto regressive models,” *Int. J. Syst. Sci.*, vol. 42, no. 9, pp. 1473–1489, 2011.
- [26] M. Chang and S. N. Pakzad, “Modified Natural Excitation Technique for Stochastic Modal Identification,” *J. Struct. Eng.*, vol. 139, no. 10, pp. 1753–1762, 2013.
- [27] T. J. Matarazzo and S. N. Pakzad, “Modal identification of golden gate bridge using pseudo mobile sensing data with STRIDE,” in *Dynamics of Civil Structures, Volume 4*, Springer, 2014, pp. 293–298.
- [28] T. J. Matarazzo and S. N. Pakzad, “STRIDE for structural identification using expectation maximization: iterative output-only method for modal identification,” *J. Eng. Mech.*, vol. 142, no. 4, p. 4015109, 2016.
- [29] J. Bendat and A. Piersol, *Engineering applications of correlation and spectral analysis*. 1993.
- [30] L. Ljung, “System Identification: Theory for the user,” *Englewood Cliffs*, 1987.
- [31] G. W. Housner and C. C. Thiel Jr., “Competing against time: report of the Governor’s Board of Inquiry on the 1989 Loma Prieta earthquake,” *Earthq. Spectra*, vol. Vol. 6, no. 4, p. 681–711. Nov., 1990.
- [32] M. Huang, P. Hipley, and A. Shakal, “Seismic Instrumentation of Toll Bridges in California,” in *Sevnetgh National Seismic Conference on Brdiges and Highways, Oakland, California, Paper*, 2013, p. P10.

- [33] S. F. Ghahari, F. Abazarsa, M. A. Ghannad, and E. Taciroglu, "Response-only modal identification of structures using strong motion data," *Earthq. Eng. Struct. Dyn.*, vol. 42, no. 8, 2013.
- [34] S. F. Ghahari, F. Abazarsa, M. A. Ghannad, M. Celebi, and E. Taciroglu, "Blind modal identification of structures from spatially sparse seismic response signals," *Struct. Control Heal. Monit.*, vol. 21, no. 5, 2014.
- [35] F. Abazarsa, F. Nateghi, S. F. Ghahari, and E. Taciroglu, "Extended blind modal identification technique for nonstationary excitations and its verification and validation," *J. Eng. Mech.*, vol. 142, no. 2, 2016.
- [36] S. F. Ghahari, F. Abazarsa, and E. Taciroglu, "Blind modal identification of non-classically damped structures under non-stationary excitations," *Struct. Control Heal. Monit.*, 2016.
- [37] François Auger, P. Flandrin, P. Gonçalvès, and O. Lemoine, "Time-Frequency Toolbox for Use with Matlab - Reference Guide," *October*, pp. 1995–1996, 1996.
- [38] M. Celebi, Y. Hisada, R. Omrani, S. F. Ghahari, and E. Taciroglu, "Responses of two tall buildings in Tokyo, Japan, before, during, and after the M9.0 Tohoku earthquake of 11 March 2011," *Earthq. Spectra*, vol. 32, no. 1, 2016.
- [39] A. Der Kiureghian, "A Coherency Model for Spatially Varying Ground Motions," *Earthq. Eng. Struct. Dyn.*, vol. 25, no. August 1995, pp. 99–111, 1996.
- [40] F. Baron, M. Arıkan, and R. E. Hamati, *The effects of seismic disturbances on the Golden Gate Bridge*. University of California, College of Engineering, Earthquake Engineering Research Center, 1976.
- [41] A. M. Abdel-Ghaffar and E. E. R. Laboratory, "Dynamic analyses of suspension bridge structures," 1976.
- [42] A. M. Abdel-Ghaffar and L. I. Rubin, "Vertical seismic behaviour of suspension bridges," *Earthq. Eng. Struct. Dyn.*, vol. 11, no. 1, pp. 1–19, 1983.
- [43] A. M. Abdel-Ghaffar and R. G. Stringfellow, "Response of suspension bridges to travelling earthquake excitations: Part I. Vertical response," *Int. J. Soil Dyn. Earthq. Eng.*, vol. 3, no. 2, pp. 62–72, 1984.
- [44] A. M. Abdel Ghaffar and L. I. Rubin, "Lateral Earthquake Response of Suspension Bridges," *J. Struct. Eng.*, vol. 109, no. 3, pp. 664–675, 1983.
- [45] A. M. Abdel-Ghaffar and R. G. Stringfellow, "Response of suspension bridges to travelling earthquake excitations: Part II-lateral response," *Int. J. Soil Dyn. Earthq. Eng.*, vol. 3, no. 2, pp. 73–81, 1984.
- [46] A. M. Abdel-Ghaffar, R. H. Scanlan, and J. Diehl, *Analysis of the dynamic characteristics of the Golden Gate Bridge by ambient vibration measurements*. Princeton University, 1985.
- [47] C. Seim and S. Rodriguez, "Seismic performance and retrofit of the Golden Gate bridge," in *Structural Engineering in Natural Hazards Mitigation*, 1993, pp. 133–138.
- [48] C. Seim and M. Ketchum, "Golden Gate Bridge Mass Transit Feasibility Study, Golden Gate Bridge, Highway and Transportation District, San Francisco, California," 1990.
- [49] S. Rodriguez and T. J. Ingham, "Seismic protective systems for the stiffening trusses of the Golden Gate Bridge," in *Proceedings of the National Seismic Conference on Bridges and Highways*, 1995.
- [50] M. Nader and T. J. Ingham, "Seismic Retrofit of the Towers of the Golden Gate Bridge," in *Proceedings of the National Seismic Conference on Bridges and Highways, San Diego, CA, December*, 1995.
- [51] R. Imbsen and R. Schamber, "Seismic retrofit of the north approach viaduct of the Golden Gate Bridge," *Transp. Res. Rec. J. Transp. Res. Board*, no. 1688, pp. 154–162, 1999.
- [52] M. I. Gürelli and C. L. Nikias, "EVAM: An Eigenvector-Based Algorithm for Multichannel Blind Deconvolution of Input Colored Signals," *IEEE Trans. Signal Process.*, vol. 43, no. 1, pp. 134–149, 1995.
- [53] Y. Nakamura, A. Der Kiureghian, and D. Liu, *Multiple-support response spectrum analysis of the Golden Gate Bridge*, vol. 93, no. 5. Earthquake Engineering Research Center, University of California, 1993.
- [54] R. A. Dameron, R. S. Dunham, and J. C. Castro, "Nonlinear analysis and experimental validation of a stiffening truss chord of the golden gate bridge," in *Computing in Civil Engineering (New York)*, 1994, no. 2, pp. 1106–1114.
- [55] T. Game *et al.*, "Full dynamic model of Golden Gate Bridge," in *AIP Conference Proceedings*, 2016, vol. 1762, no. 1, p. 20005.
- [56] Strand7, "Strand7 Finite Element Analysis System." Strand7 Software Sydney, Australia, 2007.
- [57] Hibbitt, Karlsson, and Sorensen, *ABAQUS/standard User's Manual*, vol. 1. Hibbitt, Karlsson & Sorensen, 2001.

- [58] S. V. CSI, “8, 2002. Integrated Finite Element Analysis and Design of Structures Basic Analysis Reference Manual,” *Comput. Struct. Inc., Berkeley, California, USA*, 2010.
- [59] F. McKenna, “OpenSees: a framework for earthquake engineering simulation,” *Comput. Sci. Eng.*, vol. 13, no. 4, pp. 58–66, 2011.
- [60] J. G. Reid, “Structural Identifiability in Linear Time-Invariant Systems,” *IEEE Trans. Automat. Contr.*, vol. 22, no. 2, pp. 242–246, 1977.
- [61] M. . Shrikhande and V. K. Gupta, “Dynamic soil-structure interaction effects on the seismic response of suspension bridges,” *Earthq. Eng. Struct. Dyn.*, vol. 28, no. 11, pp. 1383–1403, 1999.

